

The Bull's-Eye Effect: Are Galaxy Walls Observationally Enhanced?

Elizabeth A. Praton¹, Adrian L. Melott², and Margaret Q. McKee¹

Received _____; accepted _____

arXiv:astro-ph/9608017v2 9 Jan 1997

¹Department of Physics, Grinnell College, Grinnell, IA 50112

²Department of Physics and Astronomy, University of Kansas, Lawrence, KS 66045

ABSTRACT

We investigate a distortion in redshift-space which causes galaxies to appear to lie in walls concentric about the observer, forming a rough bull’s-eye pattern.

We simulate what an observer would see in a thin slice of redshift-space, including a magnitude limit and constant slice angle. The result is an enhanced ring of galaxies encircling the observer at a distance roughly corresponding to the peak of the selection function. This ring is an artificial enhancement of weak features in real-space. This may explain visually prominent features such as the “Great Wall” and periodicity found in deep narrow fields.

Subject headings: galaxies: distances and redshifts — large scale structure of the Universe

1. Introduction

Most maps of large scale structure use redshifts of galaxies to indicate position. Such maps are known to have distortions, the most familiar of which are the so-called fingers-of-god, elongated artifacts pointing at the observer and caused by velocities of galaxies within clusters. On scales larger than a typical finger-of-god, the maps show other features, such as great connected walls of galaxies. On these scales, are redshift-space maps essentially accurate representations of the real-space distribution? Can they be treated as fuzzy photographs of the universe?

In this paper we show that the answer may be *no*. A spectacular feature seen in redshift surveys—the curving “Great Wall” of galaxies which together with the Pisces-Perseus chain seems to form a giant ring encircling us (Geller & Huchra 1989; da Costa et al. 1994; Marzke, Huchra, & Geller 1996)—may get its visual punch from a redshift-space distortion we call the bull’s-eye effect.

Using an N-body simulation, we find that structures perpendicular to the line of sight are enhanced in redshift-space, due both to the finger-of-god distortion and a distortion caused by infall. We can further strengthen the effect by applying a magnitude limit. The result is that any observer concludes, erroneously, that he or she is encircled by galaxy walls in a bull’s-eye pattern.

2. Redshift-Space Artifacts

When peculiar velocities are small and uncorrelated, redshift maps are just fuzzier versions of real-space maps. However, large correlated velocities produce striking artifacts. One example of such an artifact is the finger-of-god produced by the random orbital motions of galaxies in a bound cluster. Another artifact, not as well known but important for this

paper, is caused by the inward flow of material toward either a single center or an extended region.

Such a flow produces an artifact because infalling material on the near-side of the accreting center or extended region has peculiar velocity away from the observer and material on the far-side has peculiar velocity toward the observer. Therefore, in redshift-space, the near-side is moved back and the far-side moved forward, squashing the material together along the radial direction. For example, studies show that spherical infall produces an extended saucer-like artifact face on to the observer, encircling the cluster finger-of-god like an outspread skirt or tutu (Kaiser 1987; Regós & Geller 1989; Praton & Schneider 1994, hereafter PS). These results are generalizable to aspherical flows. It is easy to show that *any* infall field will produce a similar artifact: see the discussion of Fig. 1 in PS.

Kaiser (1987) speculates that infall distortions may be “well able to account for” connected features seen in redshift surveys. Likewise, the schematic Fig. 6 of PS shows how an observer in a universe with many clusters might see a bull’s-eye pattern in redshift-space. More realistic scenarios than the isolated cluster model can produce an even stronger effect: bull’s-eyes are present (but uncommented on) in figures presented by Park(1990) and Ryden & Melott (1996; hereafter, RM). Weinberg & Gunn (1990a;b) comment on “hints of circular symmetry” visible in their plots (which show the effect less clearly), but attribute it to the selection function. As we will show below, the full bull’s-eye effect is a true distortion in redshift-space, and the selection function plays only a secondary role.

We wish to emphasize that walls and filaments are *real* features that arise from long-wave motion producing “pancakes” by gravitational instability (Melott & Shandarin 1990; Pauls & Melott 1995) and so do not require additional explanation such as in Kaiser (1987). On the other hand, we find that redshift effects selectively enhance pancakes

forming perpendicular to the line of sight, accelerating their apparent collapse. The toy model of an oblate spheroid may be useful here. Collapsing with its short axis along the line of sight, it may look very thin and dense in redshift space. With short axis perpendicular to the line of sight, redshift distortions make it look smaller and more nearly spherical.

3. A Simulated Universe

Before comparing redshift surveys with simulations of gravitational clustering, the two sets of data should be transformed to the same coordinate system. Observers usually work with selection effects in redshift-space, whereas simulations give complete information in real-space. Since it is presently impossible to deconvolve an observed data set to a complete real-space distribution, we must simulate realistic observational constraints, as done by Park (1990) and Weinberg & Gunn (1990 a;b).

The simulation we choose to look at is from a set of two-dimensional studies described in detail in Beacom et al. (1991) and Kauffmann & Melott (1992). RM calculated the properties of voids in three simulations in real-space and redshift-space. Of the three, the one with initial power spectrum of the form $P(k) \propto k^0$ shows the bull’s-eye effect most strongly. This index corresponds to $P(k) \propto k^{-1}$ in three dimensions, which is a reasonable approximation to the observed power spectrum over a wide range of scales (Gott & Rees 1975; Feldman, Kaiser, & Peacock 1994; Peacock & Dodds 1994; Lin et al. 1996). For these spectra, displacement varies logarithmically with k (Shandarin 1993), which can cause structure to “pile up”. The main effect of the reduced dimensionality of the simulation is the absence of the occasional very long finger-of-god due to clusters like Coma seen in the first CfA slice (de Lapparent, Geller, & Huchra 1986).

Figure 1(a) shows this simulation in real-space, and Fig. 1(b) in redshift-space, as seen

by two hypothetical observers whose positions are labeled on the plot. The simulation has periodic boundary conditions, so the figure shows the original points tiled together with copies. As in RM, we’ve first reduced the number of particles by randomly selecting one out of every four. The square has a side of approximately $600h^{-1}$ Mpc, where h is the fudge factor in the Hubble constant: $H_0 = 100h \text{ km s}^{-1} \text{ Mpc}^{-1}$, and where we let $h = 1$ for convenience. The assumed value of h affects only the selection function, not redshift displacement. The redshift-space maps made by the observers each have a radius of about $30,000 \text{ km s}^{-1}$ and overlap as indicated. Each map includes a selection function simulating the effect of a magnitude 16 limited survey.

Specifically, the luminosities of the points are assumed to obey a Schechter luminosity function: $N(> L/L_*) \propto \Gamma(1 + \alpha, L/L_*)$, where we use $\alpha = -1.07$ and $L_* = 1.0 \times 10^{10} h^{-2} L_\odot$ (e.g., Peebles 1993). We also assume that the “volume” of the observer’s sample increases with distance as in a constant angle slice. That is, we randomly select points so that the surface density at distance r goes as $\sigma \propto r \Gamma(1 + \alpha, L_0(r)/L_*)$, where $L_0(r)$ is the luminosity corresponding to the magnitude limit at the distance r .

Note that when we apply the selection function above, we essentially treat the two-dimensional simulation as if it were a three-dimensional slab. This is admittedly a swindle, but we believe a not inaccurate approximation for a thin slice. Our maps are similar in appearance to those in Park (1990), which were constructed from a three-dimensional model. Due to the high resolution of our simulation, the number of points exceeds the number of galaxies that would lie in a thin slice. Since we wish to show the origin of the effect as clearly as possible (rather than compare our results with specific surveys), we have normalized the selection function to keep all the subset simulation particles in the region of its maximum.

The difference between the real-space distribution in Fig. 1(a) and the redshift-space

maps in Fig. 1(b) is readily apparent. In the first, the distribution of “galaxies” is fairly uniform, whereas in the second, the galaxies seem to lie in curving walls which roughly circle the observer, regardless of position! Why are the two maps so different?

Figure 2 shows the simulation from the point of view of the first observer in more detail. Note: (1) The positions of the galaxies are distorted in redshift-space into smeared arclets concentric around the observer. Figure 2(a) shows the points plotted in real-space and redshift-space without the selection function. This pair of plots should be compared with Fig. 2 of RM, which shows a similar pattern appears for an observer at the center of the original square. (2) The selection effect of the magnitude limit enhances arclets at the distance where the selection function peaks. Figure 2(b) shows the real-space and redshift-space distribution of the points when the selection function is applied. This time the magnitude limit is 17, to show the effect of an increase (compare with Fig. 1). The selection function is picking out bull’s-eye rings already existing in redshift-space: it does not *produce* the pattern, as suggested by Weinberg & Gunn (1990a;b).

4. Underlying Mechanism

The mechanism underlying the bull’s-eye effect is redshift-space distortion caused by peculiar velocity. Both infall onto clusters and orbital motions within clusters contribute, as can be seen in an expanded piece of the simulation. Figure 3 shows a 20° wedge of the simulation in real-space and redshift-space, from the point of view of an observer at the center of the original square (Fig. 2 of RM) looking north. It shows several points clearly:

1. The distortion due to infall tends to empty voids and pancake galaxies on top of each other in redshift-space, perpendicular to the line of sight. Note how the two filaments on the left-hand side of the wedge between 100 and 150 Mpc are squashed together in

redshift space.

2. The finger-of-god artifacts give structures lying perpendicular to the line of sight more visual weight, by smearing the points out along the line of sight. A careful inspection of the loose filament running along the top of the wedge between 250 and 300 Mpc reveals that points are just smeared out from their positions right on top of each other. Furthermore, the fingers-of-god can be seen to be longer in dense regions with more tightly bound clumps. This correlation further increases the visual contrast.

3. The bull’s-eye pattern appears because only structures perpendicular to the line of sight are enhanced. The long filament running down the center of the wedge from 200 to 300 Mpc is not particularly enhanced in redshift-space. However, if the observer was located to the left or right of this filament, it would appear darker and thicker than it does in this view.

Again, we reiterate that the effect is caused by both the infall compression distortion and the more subtle finger of god smearing distortion. We have looked at two simulations in which one or the other distortion is suppressed. In one, small scale clustering (and thus fingers of god) are suppressed: the result is a bull’s-eye pattern which is not quite as striking as the ones shown here, rather like the figures in Weinberg & Gunn (1990a;b). In the other, peculiar velocities were reassigned randomly, removing infall: the result is a much more uniform pattern with only extremely weak suggestions of walls.

Note that the velocities in our simulation are not large. A few hundred km/s displacement is enough to produce the effect.

5. Conclusions

In the simulation examined above both motions within clusters and flows toward clusters produce distortions in redshift-space which enhance structures perpendicular to the line of sight. Redshift maps thus give the impression that the observer is surrounded by concentric walls of galaxies: the bull’s-eye effect.

It is not implausible that the bull’s-eye effect may be responsible for the visual impact of wall-like features concentric about our position, such as the Great Wall of galaxies. We would not argue that there is no physical structure underlying these features, but that existing structure may be enhanced by a simultaneous smearing and compressing distortion as in the simulation.

We note that a full view of the simulation in redshift-space shows multiple rings, separated by fairly uniform intervals. A corresponding prediction is that as the magnitude limit of magnitude complete redshift surveys is increased, other sets of walls concentric on our position but at larger distances should become apparent. Indeed, the map produced by the Las Campanas survey (Landy et al. 1996) is similar in appearance to Fig. 2(a) above. We also suggest a possible relationship to other findings based on “core-sampling” (Broadhurst et al. 1990; Doroshkevich et al. 1996; Cohen et al. 1996).

It is possible that the bull’s-eye effect is giving a misleading impression about the nature of the large scale structure of the universe. The distribution of galaxy clusters and filaments may be more uniform than impressions from redshift-space maps imply.

We wish to emphasize that our simulation only demonstrates the effect qualitatively. A detailed comparison with observational data demands the use of a three-dimensional simulation with a power spectrum more closely matched to that observed in the local universe. The spacing and intensity of this effect will depend on details of the power

spectrum and mass density of the Universe. In fact, characteristic ring spacing combined with the measured angular power spectrum should measure bulk flows and provide information on Ω_0 . Future work should include examination of the effect with a variety of three dimensional spectra and background cosmologies.

We wish to thank S. Schneider, I. Praton, S. Shandarin, D. Weinberg, and J. Gott for helpful comments. ALM wishes to acknowledge financial support from NASA Grant NAGW 3832, the NSF EPSCoR program, and Space Telescope Science Institute award number 6007.

REFERENCES

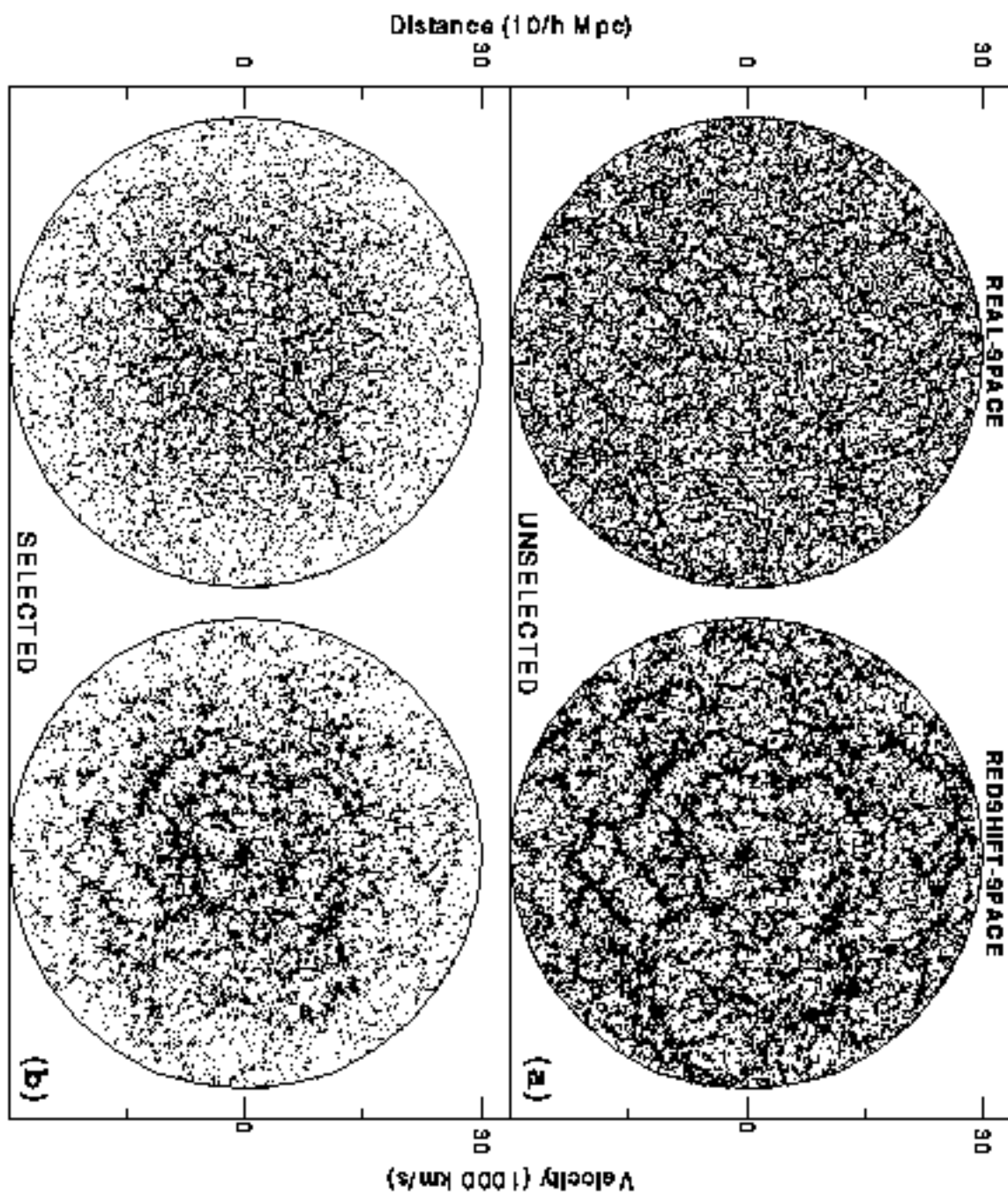
- Beacom, J. F., Dominik, K. G., Melott, A. L., Perkins, S. P., & Shandarin, S. F. 1991, *ApJ*, 372, 351
- Broadhurst, T. J., Ellis, R. S., Koo, D. C., & Szalay, A. S. 1990, *Nature*, 343, 726
- Cohen, J. L., Hogg, D. W., Pahre, M. A., & Blandford, R. 1996, *ApJ* 462, L9
- da Costa, L. N. et al. 1994, *ApJ*, 424, L1
- de Lapparent, V., Geller, M. J., & Huchra, J. P. 1986, *ApJ*, 302, L1
- Doroshkevich, A. G., Tucker, D. L., Oemler, A., Kirshner, R. P., Lin, H., Shechtman, S. A., Landy, S. D., & Fong, R. 1996, *MNRAS* in press
- Feldman, H. A., Kaiser, N., and Peacock, J. A. 1994, *ApJ*, 426, 23
- Geller, M. J., & Huchra, J. P. 1989, *Science*, 246, 897
- Gott, J. R., & Rees, M. J. 1975, *A&A*, 45, 365
- Kaiser, N. 1987, *MNRAS*, 227, 1
- Kauffmann, G., & Melott, A. L. 1992, *ApJ*, 393, 415
- Landy, S. D., Shechtman, S. A., Lin, H., Kirshner, R. P., Oemler, A. A., & Tucker, D. 1996, *ApJ*, 456, L1
- Lin, H., Kirshner, R. P., Shechtman, S. A., Landy, S. D., Oemler, A., Tucker, D. L., & Schechter, P. L. 1996, *ApJ*, 471, 617
- Marzke, R. O., Huchra, J. P., & Geller, M. J. 1996, *AJ*, 112, 1803
- Melott, A. L., & Shandarin, S. F. 1990, *Nature*, 346, 633

- Park, C. 1990, MNRAS, 242, 59p
- Pauls, J. L. & Melott, A. L. 1995, MNRAS, 274, 99
- Peacock, J. A., & Dodds, S. J. 1994, MNRAS, 267, 1020
- Peebles, P. J. E. 1993, Principles of Physical Cosmology (Princeton, NJ: Princeton University Press)
- Praton, E. A., & Schneider, S. E. 1994, ApJ, 422, 46 [PS]
- Regős, E., & Geller, M. J. 1989, AJ, 98, 755
- Ryden, B. S. & Melott, A. L. 1996, ApJ, 470, 160 [RM]
- Shandarin, S. F. 1993, Proc. Cosmic Velocity Fields, eds. F.R.Bouchet, M.Lachieze-Rey, Editions Frontieres, 383
- Weinberg, D. H., & Gunn, J. E. 1990a, ApJ, 352, L25
- Weinberg, D. H., & Gunn, J. E. 1990b, MNRAS, 247, 260

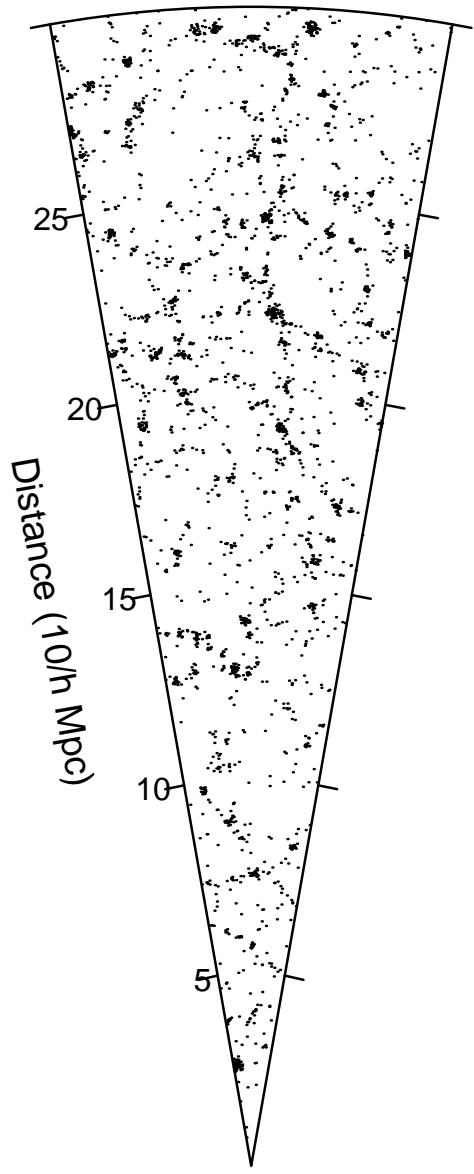
Fig. 1.— (a) A map showing the true positions of all “galaxies” and two observers in a two-dimensional simulated universe with periodic boundary conditions. The figure consists of four copies of the original set of points (inset square) tiled together. (b) The redshift-space maps made by the two observers. These maps show the velocity positions of all galaxies lying in a simulated slice with a magnitude greater than 16.

Fig. 2.— Maps of the simulation made by the first observer from Fig. 1. The observer is at the center of the circles. (a) The simulation in real-space and red-shift space, without any selection effect. (b) The simulation as seen by a survey with a magnitude limit of 17, in real-space and redshift-space.

Fig. 3.— A wedge of the simulated universe in real-space and redshift-space, as seen by an observer at the center of the inset square in Fig. 1(a).



REAL-SPACE



REDSHIFT-SPACE

